Ambipolar doping in quasifree epitaxial graphene on SiC(0001) controlled by Ge intercalation

Konstantin V. Emtsev,[1,*] Alexei A. Zakharov,[2] Camilla Coletti,[1,†] Stiven Forti,[1] and Ulrich Starke[1]
[1]*Max-Planck-Institut für Festkörperforschung, Heisenbergstrasse 1, D-70569 Stuttgart, Germany*
[2]*MAXLab, Lund University, S-22100 Lund, Sweden*

(Received 1 July 2011; revised manuscript received 12 August 2011; published 9 September 2011)

The electronic structure of decoupled graphene on SiC(0001) can be tailored by introducing atomically thin layers of germanium at the interface. The electronically inactive $(6\sqrt{3}\times 6\sqrt{3})R30^{\circ}$ reconstructed buffer layer on SiC(0001) is converted into quasi-free-standing monolayer graphene after Ge intercalation and shows the characteristic graphene π bands as displayed by angle-resolved photoelectron spectroscopy. Low-energy electron microscopy (LEEM) studies reveal an unusual mechanism of the intercalation in which the initial buffer layer is first ruptured into nanoscopic domains to allow the local in-diffusion of germanium to the interface. Upon further annealing, a continuous and homogeneous quasifree graphene film develops. Two symmetrically doped (*n*- and *p*-type) phases are obtained that are characterized by different Ge coverages. They can be prepared individually by annealing a Ge film at different temperatures. In an intermediate-temperature regime, a coexistence of the two phases can be achieved. In this transition regime, *n*-doped islands start to grow on a 100-nm scale within *p*-doped graphene terraces as revealed by LEEM. Subsequently, the *n* islands coalesce but still adjacent terraces may display different doping. Hence, lateral *p*-*n* junctions can be generated on epitaxial graphene with their size tailored on a mesoscopic scale.

DOI: 10.1103/PhysRevB.84.125423 PACS number(s): 73.22.Pr, 68.65.Pq, 73.20.At, 68.37.Nq

I. INTRODUCTION

Graphene, a single layer of sp^2-hybridized carbon atoms, is considered a highly promising electronic material due to its superior properties, including its very high charge-carrier mobility and extreme chemical inertness.[1] Epitaxial growth of graphene on single-crystal SiC wafers is considered among the most promising routes for large-scale graphene fabrication suitable for carbon-based electronics.[2–5] The recent demonstration of the half-integer quantum Hall effect, a hallmark of pristine graphene, on epitaxial graphene (EG) samples grown on either (0001) or $(000\bar{1})$ surfaces of SiC crystals proved that the substrate has no fundamental influence on the spectrum of the overlying graphene.[6,7] On SiC(0001), as-grown EG resides on top of a $(6\sqrt{3}\times 6\sqrt{3})R30^{\circ}$ reconstructed interface layer. This interface layer consists of carbon atoms in a graphenelike honeycomb arrangement. However, it has strong covalent bonds to the SiC substrate,[8,9] so that its π-band system is disrupted and does not exhibit a graphenelike electronic structure. Therefore, it is often referred to as a buffer or a zero layer (ZL). This buffer layer plays an important role in passivating the dangling bonds of the SiC substrate, so that overlying graphene layers exhibit truly delocalized π orbitals.[3,4,8] The interface, however, contains a high density of surface states that induce a very high electron doping level in the range of $1\times 10^{13}\,\mathrm{cm}^{-2}$. Charged interface states are also believed to act as scattering centers responsible for a reduced mobility of charge carriers in EG as compared to exfoliated graphene flakes. An elegant way to circumvent the influence of this interface was recently demonstrated by passivating the interface states with hydrogen.[10] Upon hydrogen intercalation, the buffer layer is relieved from the substrate and turns into quasi-free-standing graphene as the formerly covalent bonds are broken and all Si atoms of the SiC are saturated with hydrogen. Alternatively, noble metals have been used for atomic intercalation underneath graphene on transition metals, a process that leads to substantial weakening of the graphene-substrate interaction.[11,12] It was also shown that a monolayer (ML) of gold atoms can be intercalated in between the graphene and the $(6\sqrt{3}\times 6\sqrt{3})R30^{\circ}$ buffer layer[13,14] or between SiC and a bare buffer layer.[15] In the latter case, too, the buffer layer is lifted off the substrate and assumes graphene electronic properties. However, in these studies, the gold layer displays a significant interaction with the EG-SiC system by forming ordered structures, e.g., a (2×2) phase, a $(2\sqrt{3}\times 2\sqrt{3})R30^{\circ}$ phase, or a Moire pattern. Moreover, the presence of metallic states underneath graphene would be disadvantageous considering perspective applications of graphene in electronic devices. In this respect, intercalation of nonmetallic atomic layers would be preferable. Ge, for example, shows a notable interaction with graphite sheets on SiC(0001) as observed by low-energy electron diffraction (LEED) and x-ray photoelectron spectroscopy (XPS).[16] It was shown that upon annealing, initially three-dimensional Ge droplets were transformed into two-dimensional layers. A diffusion under the graphene sheets was suggested. It should be very interesting, therefore, to explore the electronic structure of EG on SiC(0001) after thermal reaction with Ge.

In the present work, we show that by processing a $(6\sqrt{3}\times 6\sqrt{3})R30^{\circ}$ reconstructed SiC(0001) surface (ZL) with different amounts of Ge, the Ge indeed intercalates between the ZL and the SiC(0001) substrate. After annealing the Ge-covered sample, the π bands characteristic for graphene develop where before the ZL was electronically inactive. Most interestingly, the electronic structure of the resulting decoupled graphene layer can be tailor-made. Two symmetrically doped (*n*- and *p*-type) phases are obtained depending on the preparation conditions. Moreover, a coexistence of the two phases within the graphene sample is possible, so that the engineering of lateral *p*-*n* junctions can be attempted. *p*-*n* junctions in graphene are indeed expected to exhibit some very peculiar properties such as Klein tunneling[17] or

 ©2011 American Physical Society

unconventional electron focusing and lensing as predicted recently.[18] In our experiments, LEED and XPS results manifest the decoupling of the $(6\sqrt{3} \times 6\sqrt{3})R30^\circ$ layer from the SiC(0001) substrate after Ge deposition and annealing. The π bands are monitored directly by angle-resolved photoelectron spectroscopy (ARPES) in the vicinity of the $\bar{\mathrm{K}}$ point of the graphene Brillouin zone. The microscopic details of the intercalation process are observed *in situ* using low-energy electron microscopy (LEEM) and photoelectron microscopy (PEEM). The nucleation of n-type inclusions in p-type layers is monitored *in situ* on a mesoscopic scale proceeding from nanosized islands to the complete transformation of terraces.

II. EXPERIMENT

The initial $(6\sqrt{3} \times 6\sqrt{3})R30^\circ$ reconstructed SiC(0001) surfaces were prepared either by annealing of the samples at $T = 1100$ °C in an ultrahigh-vacuum (UHV) chamber[19] or at $T = 1400$ °C in an rf furnace under an argon atmosphere.[5] We note that the principal difference between the two methods lies in the size of the produced single-domain buffer layer areas that are of the order of several micrometers for the rf and only ~ 100 nm for the UHV method.[5] In addition, the surface morphology of the argon grown samples is significantly smoother. We note also that the band engineering reported below does not depend on the growth method used. Deposition of up to five ML germanium on the $(6\sqrt{3} \times 6\sqrt{3})R30^\circ$ reconstructed SiC(0001) surface was carried out in UHV using a Knudsen cell. Subsequently, the samples were annealed at temperatures between 600 and 1100 °C while the intercalation process was monitored by LEED and XPS. The samples were characterized by high-resolution ARPES using a Scienta SES-2002 electron analyzer at the SIS-HRPES beamline of the Swiss Light Source at the Paul Scherrer Institute (Villigen, Switzerland). LEEM and PEEM as well as μ-LEED and μ-XPS experiments using the Elmitec-SPELEEM III instrument were carried out at beamline I311 at the MAX Radiation Laboratory (Lund, Sweden).

III. RESULTS AND DISCUSSION

A. Structural and electronic decoupling of the graphene layer

The as-grown buffer layer displays a typical $(6\sqrt{3} \times 6\sqrt{3})R30^\circ$ LEED pattern as shown in Fig. 1(a). It contains sharp spots of the SiC substrate and the graphenelike carbon adlayer together with intense superstructure spots that reflect the large commensurate reconstruction of the adlayer on top of the SiC(0001) surface.[4,8] The buffer layer is aligned with respect to the SiC substrate with a mutual rotation angle of 30°. The chemical bonding of the buffer layer is revealed in the C 1s core-level spectrum in Fig. 1(b), which—in addition to the SiC bulk peak—exhibits two components that correspond to carbon atoms in the buffer layer with (S1) and without (S2) chemical bond to the SiC substrate, respectively.[8] Drastic changes in ordering and chemical composition of the surface take place after deposition and annealing (700–900 °C) of a few atomic layers of germanium, as shown in Figs. 1(c) and 1(d). Annealing to 720 °C after deposition of 5 ML of Ge

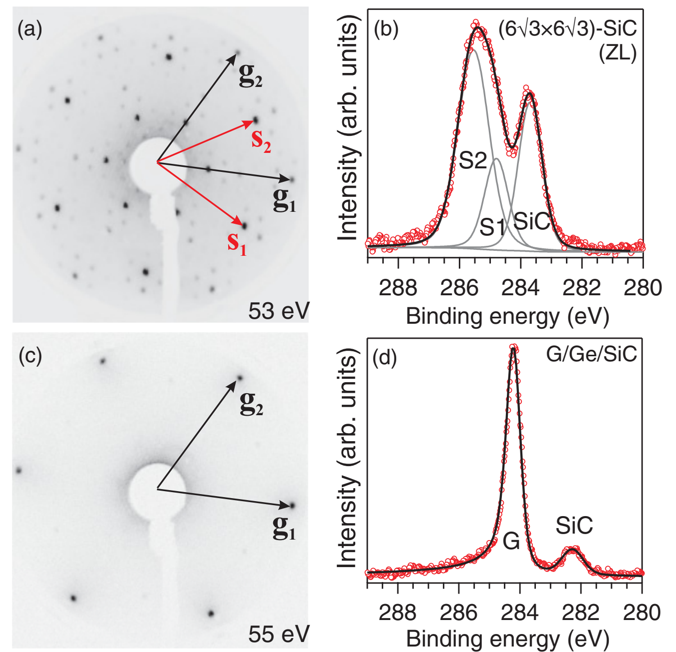

FIG. 1. (Color online) (a,c) LEED patterns and (b,d) C 1s core-level spectra taken from the initial $(6\sqrt{3} \times 6\sqrt{3})R30^\circ$ reconstructed SiC(0001) surface (a,b) and after deposition of 5 ML of Ge followed by vacuum annealing at $T = 720$ °C (c,d). In the LEED images, the reciprocal-lattice vectors of the SiC and graphene lattices are indicated as (s_1,s_2) and (g_1,g_2), respectively. The C 1s core-level spectra were acquired using a photon energy of 380 eV. Experimental data are shown as open (red) dots, fitted by the solid (black) lines. In panel (b), the fitted components are also shown (gray lines).

results in a complete disappearance of the initial $(6\sqrt{3} \times 6\sqrt{3})R30^\circ$ reconstruction, as is evident from the LEED pattern in Fig. 1(c). Even the (1×1) spots of the unreconstructed SiC substrate are strongly suppressed so that often only the graphene diffraction pattern remains visible, in agreement with earlier data.[16] The nature of the structural transformation can be seen by comparing the C 1s core-level spectra in Fig. 1(d) with those in panel (b). The components S1 and S2 of the $(6\sqrt{3} \times 6\sqrt{3})R30^\circ$ layer are now converged into a single sharp peak (G) resembling that of pristine sp^2-hybridized carbon. In contrast to the initial surface, all carbon atoms of the overlayer are now in the same chemical bonding state. Note also that the signal of the SiC substrate is significantly damped in comparison to the initial surface. The above structural data can be reconciled in a model where Ge atoms diffuse underneath the $(6\sqrt{3} \times 6\sqrt{3})R30^\circ$ buffer layer and thereby break its covalent bonds to the Si atoms of the SiC substrate. The lack of chemically shifted components in the C 1s core-level spectrum after such an intercalation indicates that Ge atoms located now at the interface do not interact covalently with the carbon atoms of the buffer layer. As is evident from LEED, the interfacial germanium layer does not induce a long-range reconstruction of the graphene lattice in contrast to other intercalated graphene systems.[12–15] Hence, the graphene buffer layer becomes structurally decoupled from the SiC substrate upon intercalation of Ge atoms.

In Fig. 2, the electronic band structure around the $\bar{\mathrm{K}}$ point of the graphene Brillouin zone is shown for different stages of

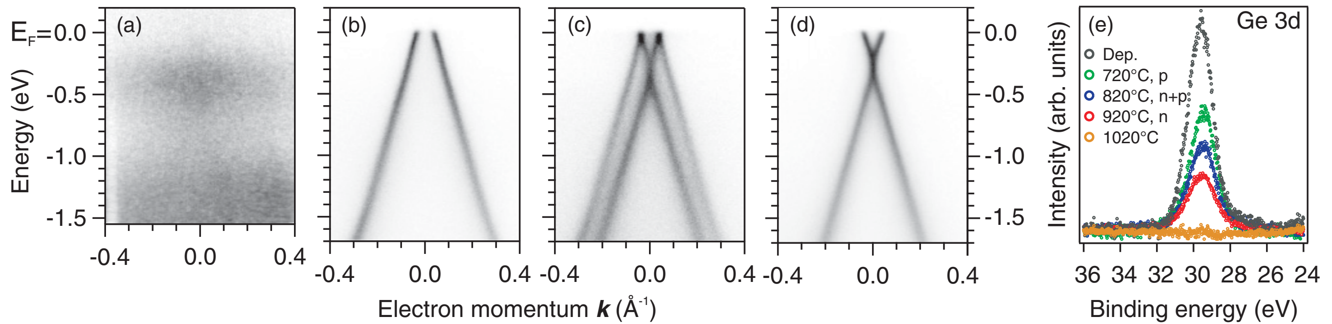

FIG. 2. (Color online) (a)–(d) Photoemission valence-band maps vs energy and electron momentum in the vicinity of the $\bar{\mathrm{K}}$ point ($\mathbf{k} = 0$) of the graphene Brillouin zone taken from (a) the initial $(6\sqrt{3} \times 6\sqrt{3})R30^{\circ}$ surface and after deposition of 5 ML of Ge followed by vacuum annealing at (b) $T = 720$ °C, (c) 820 °C, and (d) 920 °C. The photon energy was 90 eV. (e) XPS Ge $3d$ core-level spectra obtained after deposition and for different annealing temperatures (top down). The intensities are normalized with respect to the substrate Si $2p$ emission. The graphene doping indicated corresponds to the data shown in panels (b)–(d). The photon energy was 1253.6 eV.

the intercalation and annealing process. As noted above, the initial $(6\sqrt{3} \times 6\sqrt{3})R30^{\circ}$ buffer layer shows no graphenelike π bands, as seen in Fig. 2(a).[8] Intercalation of germanium at the interface with SiC [Fig. 2(b)] leads to the appearance of sharp π bands as expected for pristine graphene. We find that depending on the preparation conditions (differences in the initial Ge coverage or annealing temperature), the decoupled graphene exhibits two stable phases characterized by p- or n-type doping, cf. Figs. 2(b) and 2(d). At an annealing temperature of $T = 720$ °C as used for the data shown in Fig. 1, graphene exhibits a hole doping of $p = 4.1 \times 10^{12}\mathrm{cm}^{-2}$ while a further increase of the annealing to $T = 920$ °C inverts the doping to an electron type with a concentration of $n = 4.8 \times 10^{12}$ cm^{-2}. As judged from the Ge $3d$ core-level spectra observed in XPS, cf. Fig. 2(e), annealing to 720 °C and temperatures above is accompanied by a gradual loss of germanium from the surface until it vanishes above 1020 °C. Hence, the two phases should correspond to different amounts of intercalated Ge atoms. Indeed, both phases can be prepared at the same temperature of $T = 720$ °C simply by varying the initial germanium coverage. Quantification of the corresponding XPS spectra shows that the n phase is induced upon intercalation of approximately one monolayer (ML) of Ge atoms (for Ge, 1 ML $= 7.4 \times 10^{14}$ cm^{-2}) while about 2 ML of Ge are required in order to produce p-type graphene. At the same time, we note that the probability of the intercalation is not 100%. So, deposition of Ge corresponding to around 3-ML thickness results in n-type graphene after intercalation, while thicker films lead to a p-type doping. Presumably during the annealing process, Ge partially sublimates from the surface and/or agglomerates into Ge particles on top. Interestingly, a coexistence of the p- and n-doped graphene band structures, i.e., of p- and n-doped graphene regions on the surface, can be generated at intermediate temperatures, as shown in Fig. 2(c). At this temperature, an intermediate Ge content is found in XPS, cf. Fig. 2(e). This observation implies that a lateral structuring of p-n junctions can be induced in epitaxial graphene by controlling the composition of the interface. Moreover, the p-n junctions induced by a varying degree of Ge intercalation display a nearly symmetric charge distribution [see Fig. 2(c)]. The reason for the development of the two distinct phases can only lie in the different thickness of the interfacial Ge layer. A doping effect of Ge droplets can be ruled out, since droplets are only occasionally present on top of graphene as controlled by monitoring possible oxidation in the Ge $3d$ core level after exposing the samples to ambient conditions. Also, a covalent interaction of the Ge with the graphene layer is absent as judged from the C $1s$ core-level spectra. The doping of graphene layers, however, has been predicted to depend on the spacing from adjacent metal layers[20] corroborating our interpretation.

B. Microscopic study of Ge intercalation

In order to understand the microscopic picture of the intercalation process, the transition was monitored *in situ* using LEEM. LEEM micrographs taken before and after the intercalation process are shown in Figs. 3(a) and 3(b). The $(6\sqrt{3} \times 6\sqrt{3})R30^{\circ}$ reconstructed graphene layer of the initial sample extends homogeneously over the surface terraces as a result of the Ar furnace annealing process.[5] The terraces are of the order of several micrometers in width. Only very small inclusions (<3%) of ML graphene [dark gray lines in Fig. 3(a)] are observed nucleating on top of the buffer layer along the terrace step edges.[5] After the intercalation [Fig. 3(b)], the appearance of the surface remains principally unchanged as far as the microstructure of the terraces is concerned. Decoupled graphene is seen to be continuous and homogeneous over the entire surface. At the same time, the LEEM I-V electron reflectivity curves[21,22] shown in Fig. 3(c) clearly demonstrate the development of a quasifree graphene monolayer upon intercalation. While the initial $(6\sqrt{3} \times 6\sqrt{3})R30^{\circ}$ surface has a fairly flat featureless spectrum, the decoupled layer exhibits a dip in the electron reflectivity at energies between 2 and 3 eV as expected for ML graphene.[10,21,22] The similarity of spectra obtained from different terraces on the sample [boxes shown in panels (a) and (b)] corroborates the homogeneity of the decoupled graphene layer. We also note that the I-V curve of the Ge-intercalated graphene has a second dip at a higher energy of around 7 eV. This dip is not present in the case of as-grown monolayer graphene on SiC(0001),[21] and, therefore, should be specific to the atomic and/or electronic structure of the new interface.

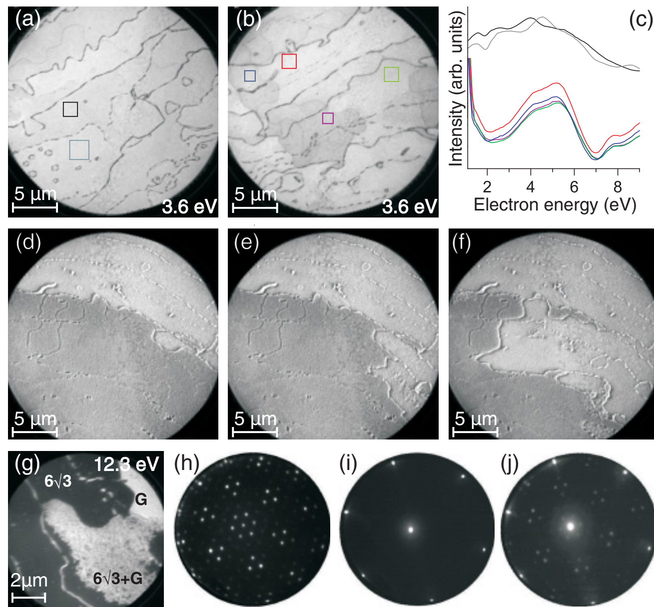

FIG. 3. (Color online) LEEM micrographs of (a) the initial $(6\sqrt{3}\times 6\sqrt{3})R30^{\circ}$-SiC(0001) surface and (b) quasifree standing graphene obtained by intercalation of Ge atoms. (c) LEEM reflectivity curves collected from different areas of the initial surface (upper curves) and of the Ge intercalated graphene (lower curves) as indicated by squares in (a) and (b). (d)–(f) LEEM micrographs obtained during the transformation at 720 °C with ≈30 s difference. (g) LEEM micrograph of the quenched surface, i.e., after incomplete intercalation imaged with a smaller field of view. (h)–(j) μ-LEED snapshots (43 eV) of the dark, bright, and grainy areas of panel (g), corresponding to an unconverted Ge covered surface $6\sqrt{3}$, a fully converted graphene phase (**G**), and a partially converted area ($6\sqrt{3}+\mathbf{G}$) quenched in the transformation process, respectively.

In order to gain insight into the mechanism of the germanium penetration underneath the $(6\sqrt{3}\times 6\sqrt{3})R30^{\circ}$ layer, LEEM images were acquired *in situ* during the annealing process. The series of micrographs in Figs. 3(d)–3(f) shows that the intercalation process proceeds fast over a complete terrace, while at the terrace edges it appears to be kinetically limited until an initiating transformation step occurs. A movie sequence of the transformation can be found in the supplemental material.[23] The surface was quenched during the intercalation process in order to reveal the microscopic details of the transformation. A characteristic image of the incomplete intercalation process is shown in Fig. 3(g). The micrograph displays three characteristic areas, which are distinguished by the contrast and can be identified by the μ-LEED snapshots in Fig. 3. The dark area corresponds to an unconverted surface (covered with Ge) as it shows the full $(6\sqrt{3}\times 6\sqrt{3})R30^{\circ}$ reconstruction [panel (h)]. The bright area is fully converted and shows only the graphene diffraction pattern [panel (i)]. The image in panel (j) is obtained from the grayish grainy area and displays a superposition of the $(6\sqrt{3}\times 6\sqrt{3})R30^{\circ}$ and the (1×1) graphene diffraction patterns. That indicates the presence of an inhomogeneous transition phase, which is different from either the initial surface or a fully developed graphene film. The transition region consists of densely packed grains of $\sim$50 nm in size. Presumably, the grains are small areas where the germanium is already intercalated and is covered with graphene islands. With time these intercalation seeds anneal out and gradually coalesce into a continuous graphene layer when the transformation is completed, cf. Fig. 3(b). This suggests that the intercalation process proceeds by rupturing the domains of the initial $(6\sqrt{3}\times 6\sqrt{3})R30^{\circ}$ layer, which provides a pathway for local in-diffusion of germanium to the interface. In such a way, no macroscopic diffusion of germanium takes place, in contrast to conventional intercalation processes in graphite. At the same time, the mobility of carbon species on top of the germanium layer is high and allows complete healing of the graphene grains. Apparently, this intercalation mechanism is favored on the buffer layer graphene due to its higher chemical reactivity with respect to that of pristine graphene. Indeed, the presence of a significant number of sp^3-like coordinated carbon atoms makes the layer more susceptible for chemical reactions. Similarly, structural corrugations of graphene such as ripples are believed to be more reactive to chemisorption as compared to a flat graphene.[24]

As described in the previous section, further annealing reverts the doping of graphene from p- to n-type. This process coincides with a partial loss of germanium from the surface as observed by XPS, i.e., a partial deintercalation. The mixed p/n phase appears to be particularly interesting as it represents a coexistence of lateral graphene p-n junctions on the surface. In Fig. 4, we compare the LEEM micrographs taken at the same position on the sample of the initial p-phase graphene [panel (a)] and after nucleation of the n-phase graphene upon annealing to 820 °C [panel (b)]. Surprisingly, the process is not initiated at the step edges but rather on the terraces as seen in Fig. 4(b). Islands of the n-doped graphene that are roughly circular in shape appear to be embedded in the p-doped graphene terraces. At the beginning of the process, they have sizes of 100 nm or less.

The lack of preferential desorption of germanium atoms from the step edges during de-intercalation is rather unusual. Graphene flakes of limited size generally show different behavior in which (de)intercalation commences at the edge of the flake.[25] This is so since the diffusion coefficients for intercalants along the basal plane are generally several orders of magnitude higher than those perpendicular to graphene planes.[26] The latter requires formation of substitutional sites (point defects) in the graphene plane, which is energetically much more costly. In fact, we find that the eventual pattern of p-n areas depends to some extent on the cooling speed, which supports the idea that Ge atoms are mobile underneath graphene at quite low temperatures. Apparently, after completion of the intercalation process [p phase in Fig. 3(b)], no germanium out-diffusion is allowed at the steps, which suggests continuity of the free-standing graphene islands over the neighboring terraces. This is also supported by the occasional observations of strain relaxation pleats in the decoupled graphene film formed after cooling that in many cases run across substrate steps (not shown). Hence, our data point toward a model in which the loss of germanium at temperatures above 800 °C occurs via the formation of Ge interstitial sites in the graphene lattice (a process that is probably facilitated by the presence of point defects in

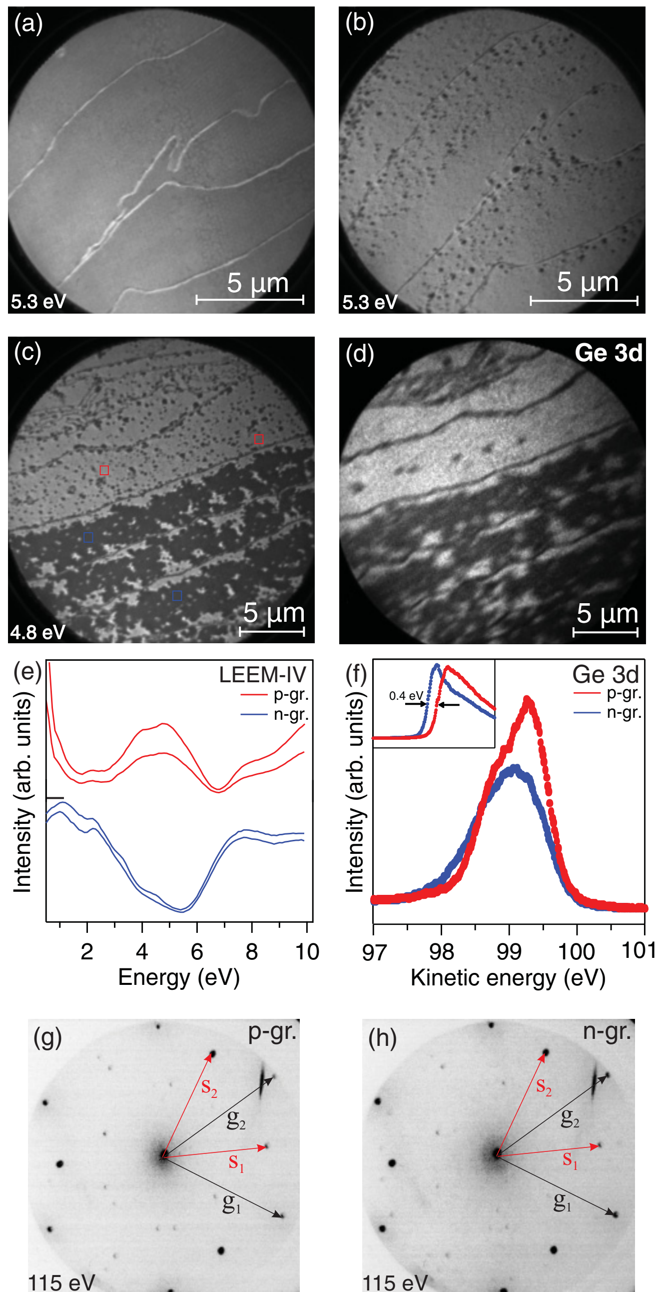

FIG. 4. (Color online) Formation of graphene *p*-*n* junctions by partial deintercalation of germanium atoms from the interface with the SiC(0001) surface: (a,b) LEEM micrographs of the same area on the sample taken before and after nucleation of the *n*-doped graphene phase upon annealing at $T = 820\ ^\circ$C. Dark inclusions in (b) correspond to the *n*-doped graphene islands embedded into the *p*-doped graphene sheet. (c,d) LEEM micrograph and PEEM Ge 3*d* intensity map taken at a later stage of the graphene *n*-phase formation. Bright (dark) regions in (c,d) correspond to *p*-doped (*n*-doped) graphene regions. (e,f) LEEM reflectivity curves and Ge 3*d* core levels taken from the *p*- and *n*-doped regions shown in (c) and (d), respectively. The inset in (f) shows the low-energy cutoff of the PEEM signals indicating the work-function shift for the two phases. (g,h) μ-LEED patterns of the *p*- and *n*-doped graphene areas. The reciprocal-lattice vectors of the SiC and graphene lattices are indicated as (s_1,s_2) and (g_1,g_2), respectively.

graphene such as vacancies) with their subsequent sublimation from the surface. It must be expected that such a process generates defects in the *n*-doped graphene areas. STM studies would help to resolve these questions.

As the annealing temperature increases, the *n*-doped areas grow in size and begin to coalesce, thus forming extended regions as shown in Fig. 4(c) taken at a later stage of deintercalation. A PEEM micrograph of the Ge 3*d* core level taken at the same location is shown in Fig. 4(d). There is a significant contrast in intensity of the Ge 3*d* core-level signals [the corresponding Ge 3*d* core-level spectra are shown in Fig. 4(f)] for the two graphene phases, and hence the amount of germanium located underneath the graphene layer is notably different. Apparently, the *n* phase is characterized by a thinner interfacial Ge layer than the *p* phase, which is in accordance with the XPS data given in the previous section. The equivalence of the surface features imaged in PEEM and LEEM is quite obvious in Figs. 4(c) and 4(d). Moreover, the same contrast as in Figs. 4(c) and 4(d) was obtained in the PEEM work-function mapping. Indeed, the low-energy cutoffs taken from the two phases shown in the inset of Fig. 4(f) exhibit a relative shift of ~0.4 eV at the *p*-*n* interface, as expected from the difference in doping between *p*- and *n*-doped regions (see Fig. 2).

The LEEM reflectivity curves taken from both phases are shown in Fig. 4(e) together with their μ-LEED patterns in Figs. 4(g) and 4(h). In the low-energy regime, the *I*-*V* curves are quite distinct, which makes the identification of the corresponding areas in LEEM micrographs simple. As discussed above, the *p*-doped quasi-free-standing graphene shows a dip at an energy around 2.6 eV as expected based on the model proposed by Hibino *et al.*[21] The *I*-*V* curve of the *n* phase is rather distinct and shows a dip at significantly higher energy of ~5 eV that cannot be described by the model.[21] Obviously, the reflectivity of the surface at such low energies is sensitive not only to the band structure of the graphene but also to the electronic and atomic structure of the interface. We note that this is also the case for graphene on Pt(111) despite the weak graphene substrate interaction.[27]

Remarkably, very little difference between the two phases is observed in the μ-LEED patterns, as can be seen in Figs. 4(g) and 4(h). In addition to the (1×1) diffraction spots corresponding to SiC and graphene, we observe fractional order spots of the $(6\sqrt{3} \times 6\sqrt{3})R30^\circ$ periodicity, however much weaker than for the initial, reconstructed surface [compare to Fig. 1(a)]. These spots can be attributed to the double diffraction of electrons at the atomic potential of the substrate and the graphene lattice. They are inherent for any epitaxial SiC-graphene system with the $(6\sqrt{3} \times 6\sqrt{3})R30^\circ$ registry of substrate and adlayer due to the strong scattering cross section of low-energy electrons.[4] In the present case, however, they appear very weak due to additional attenuation by the germanium layer. As we can also see from the μ-LEED patterns, the interfacial Ge layer does not produce any additional reconstruction in either case.

IV. CONCLUSION

In conclusion, ultrathin germanium buffer layers can be introduced at the interface between the $(6\sqrt{3} \times 6\sqrt{3})R30^\circ$-

reconstructed layer and the SiC(0001) surface by atomic intercalation. The dilated interface decouples the $(6\sqrt{3} \times 6\sqrt{3})R30^{\circ}$ layer from the SiC surface and recovers the electronic structure of graphene. A quasi-free-standing graphene monolayer develops and shows moderate p or n doping depending on the amount of Ge intercalated. The transformation from the p- to the n-doped phase develops on a 100-nm scale so that mesoscopic lateral p-n junctions can be fabricated on epitaxial graphene.

ACKNOWLEDGMENTS

C.C. acknowledges the Alexander von Humboldt Foundation for financial support. This research was partially funded by the European Community's Seventh Framework Programme: Research Infrastructures (FP7/2007-2013) under Grant agreement No. 226716. We are indebted to the staff at MAX-Lab (Lund, Sweden) and SLS (Villigen, Switzerland) for their advice and support.

[*]k.emtsev@fkf.mpg.de; [http://www.fkf.mpg.de/ga]

[†]Present address: Center for Nanotechnology Innovation @ NEST, Istituto Italiano di Tecnologia, 56127 Pisa, Italy.

[1]A. K. Geim and K. S. Novoselov, Nat. Mater. **6**, 183 (2007).

[2]C. Berger, Z. Song, X. Li, X. Wu, N. Brown, C. Naud, D. Mayou, T. Li, J. Hass, A. N. Marchenkov, E. H. Conrad, P. N. First, and W. A. de Heer, Science **312**, 1191 (2006).

[3]T. Ohta, A. Bostwick, J. L. McChesney, Th. Seyller, K. Horn, and E. Rotenberg, Phys. Rev. Lett. **98**, 206802 (2007).

[4]C. Riedl, A. A. Zakharov, and U. Starke, Appl. Phys. Lett. **93**, 033106 (2008).

[5]K. V. Emtsev, A. Bostwick, K. Horn, J. Jobst, G. L. Kellogg, L. Ley, J. L. McChesney, T. Ohta, S. A. Reshanov, J. Röhrl, E. Rotenberg, A. K. Schmidt, D. Waldmann, H. B. Weber, and T. Seyller, Nat. Mater. **8**, 203-207 (2009).

[6]J. Jobst, D. Waldmann, F. Speck, R. Hirner, D. K. Maude, T. Seyller, and H. B. Weber, Phys. Rev. B **81**, 195434 (2010).

[7]P. N. First, W. A. de Heer, T. Seyller, C. Berger, J. A. Stroscio, and J-S. Moon, MRS Bull. **35**, 296 (2010).

[8]K. V. Emtsev, F. Speck, T. Seyller, L. Ley, and J. D. Riley, Phys. Rev. B **77**, 155303 (2008).

[9]C. Riedl, C. Coletti, and U. Starke, J. Phys. D **43**, 374009 (2010).

[10]C. Riedl, C. Coletti, T. Iwasaki, A. A. Zakharov, and U. Starke, Phys. Rev. Lett. **103**, 246804 (2009).

[11]Yu. S. Dedkov, A. M. Shikin, V. K. Adamchuk, S. L. Molodtsov, C. Laubschat, A. Bauer, and G. Kaindl, Phys. Rev. B **64**, 035405 (2001).

[12]A. Varykhalov, J. Sanchez-Barriga, A. M. Shikin, C. Biswas, E. Vescovo, A. Rybkin, D. Marchenko, and O. Rader, Phys. Rev. Lett. **101**, 157601 (2008).

[13]B. Premlal, M. Cranney, F. Vonau, D. Aubel, D. Casterman, M. M. De Souza, and L. Simon, Appl. Phys. Lett. **94**, 263115 (2009).

[14]M. Cranney, F. Vonau, P. B. Pillai, E. Denys, D. Aubel, M. M. De Souza, C. Bena, and L. Simon, Europhys. Lett. **91**, 66004 (2010).

[15]I. Gierz, T. Suzuki, R. T. Weitz, D. S. Lee, B. Krauss, C. Riedl, U. Starke, H. Höchst, J. H. Smet, C. R. Ast, and K. Kern, Phys. Rev. B **81**, 235408 (2010).

[16]L. Kubler, K. Aït-Mansour, M. Diani, D. Dentel, J.-L. Bischoff, and M. Derivaz, Phys. Rev. B **72**, 115319 (2005).

[17]M. I. Katsnelson, K. S. Novoselov, and A. K. Geim, Nat. Phys. **2**, 620 (2006).

[18]V. V. Cheianov, V. Fal'ko, and B. L. Altshuler, Science **315**, 1252 (2007).

[19]C. Riedl, U. Starke, J. Bernhardt, M. Franke, and K. Heinz, Phys. Rev. B **76**, 245406 (2007).

[20]G. Giovannetti, P. A. Khomyakov, G. Brocks, V. M. Karpan, J. van den Brink, and P. J. Kelly, Phys. Rev. Lett. **101**, 026803 (2008).

[21]H. Hibino, H. Kageshima, F. Maeda, M. Nagase, Y. Kobayashi, and H. Yamaguchi, Phys. Rev. B **77**, 075413 (2008).

[22]T. Ohta, F. El Gabaly, A. Bostwick, J. L. McChesney, K. V. Emtsev, A. K. Schmid, T. Seyller, K. Horn, and E. Rotenberg, New J. Phys. **10**, 023034 (2008).

[23]See Supplemental Material at http://link.aps.org/supplemental/10.1103/PhysRevB.84.125423. LEEM movie sequence of the quasifree standing graphene formation by intercalation of Ge atoms underneath the buffer layer graphene on SiC(0001) surface. The transition takes place at $T = 720^{\circ}$ C.

[24]D. W. Boukhvalov and M. I. Katsnelson, J. Phys. Chem. C **113**, 14176 (2009).

[25]P. Sutter, J. T. Sadowski, and E. Sutter, J. Am. Chem. Soc. **132**, 8175 (2010).

[26]I. Suarez-Martinez, A. A. El-Barbary, G. Savini, and M. I. Heggie, Phys. Rev. Lett. **98**, 015501 (2007).

[27]P. Sutter, J. T. Sadowski, and E. Sutter, Phys. Rev. B **80**, 245411 (2009).